

Dual nature of a charge-density-wave transition on In/Cu(001)

T. Nakagawa,* H. Okuyama, M. Nishijima, and T. Aruga[†]

Department of Chemistry, Graduate School of Science, Kyoto University, Kyoto 606-8502, Japan

H. W. Yeom

Atomic-scale Surface Science Research Center and Department of Physics, Yonsei University, Seoul 120-749, Korea

E. Rotenberg

Advanced Light Source (ALS), Ernest Orlando Lawrence Berkeley National Laboratory, Berkeley, California 94720, USA

B. Krenzer and S. D. Kevan

Department of Physics, University of Oregon, Eugene, Oregon 97403, USA

(Received 7 March 2003; published 10 June 2003)

A surface phase transition on In/Cu(001) with In coverage of 0.63 was studied. The structural analysis shows that the reversible phase transition at 405 K between the high-temperature (2×2) and the low-temperature ($2\sqrt{2} \times 2\sqrt{2}$) $R45^\circ$ phases belongs to an order-disorder type. The angle-resolved photoemission experiment shows that the low-temperature phase is stabilized by the partial gap formation at the Fermi surface, indicating that the transition is due to the Peierls-type Fermi-surface nesting. While the above observations point to a strong-coupling charge-density-wave (SCDW) scenario, the temperature-dependent behavior of the gap is in better agreement with the weak-coupling CDW theory. Thus, the results serve the first experimental characterization of the CDW transition driven cooperatively by electronic and lattice entropies.

DOI: 10.1103/PhysRevB.67.241401

PACS number(s): 73.20.At, 68.35.Bs, 71.45.Lr

Phase transitions in ultrathin films have attracted growing interest since the report of a two-dimensional (2D) charge-density-wave (CDW) transition on Pb/Ge(111).¹ The works in such class of materials are motivated in part by their potential importance in the materials physics in nanometer scale.

The current view of the CDW transitions in quasi-low-dimensional systems is well documented in the literature.²⁻⁵ It is important to classify the CDW's according to the strength of the electron-phonon (e -ph) coupling, which determines crucially the characteristics of the transitions. (The difference between weak- and strong-coupling CDW's has often been dismissed in the studies of surface CDW's, which in some cases resulted in unnecessary confusion.) At nonadiabatic limit, the weak e -ph coupling causes a small (less than a characteristic phonon energy, i.e., several tens of meV) band gap at the Fermi level, which stabilizes the CDW state if the electronic energy gain due to the gap formation overcomes the loss in elastic energy. Upon raising the temperature, the thermal excitation of electrons across the band gap degrades the CDW stability and eventually drives the system to a normal-metal state, in which the band crosses the Fermi level and constitutes the Fermi surface (FS). The structural transition in this case should be categorized into a displacive type. On the other hand, for adiabatic CDW's with a strong e -ph coupling,^{4,6,7} the phase fluctuation of the frozen-in phonon mode sets in, with its amplitude being still large, at a temperature well below that required for the electronic excitation across the gap. This leads the free-energy surface to have a multimimum shape, and the system to undergo an order-disorder-type phase transition. In this case, the electronic structure in both the low-temperature (LT) and the high-temperature (HT) phases should be well described

in terms of a local-bonding picture. The band gap, which corresponds to a bonding-antibonding splitting in the chemical-bond language, is hence expected to be maintained in the HT phase.

The understanding of any CDW transition should, hence, be based on the knowledge of both geometric and electronic structures. For surface transitions, the former can be studied by complementary means: structure factors in reciprocal space by low-energy electron diffraction (LEED) and real-space arrangements of individual atoms by scanning-tunneling microscopy (STM). As to the electronic structure, angle-resolved photoelectron spectroscopy (ARPES) can reveal the complete band structure of 2D systems, and has been applied to several quasi-1D and quasi-2D CDW systems.⁸⁻¹⁵ The works for the incommensurate CDW phase in SmTe₃ (Ref. 8) and a commensurate one on In(0.5 ML)/Cu(001) (Ref. 14) showed imperfect nesting of the Fermi surface and the gap anisotropy in momentum space, ML represents monolayer.

In this paper, we show the combined experimental results for a phase transition on the In(0.63 ML)/Cu(001) surface. The results of LEED and STM show that the transition is unambiguously of order-disorder-type and ARPES shows directly a large CDW gap in LT phase. These results imply that the transition is driven by the lattice entropy and should be categorized into short-coherence-length strong-coupling CDW (SCDW).⁶ However, the temperature-dependent measurement of the gap shows that the gap decreases with increasing temperature and disappears at the transition temperature, which is a characteristic behavior for weak-coupling CDW's (WCDW's). Thus, the CDW transition cannot be classified only according to the strength of the

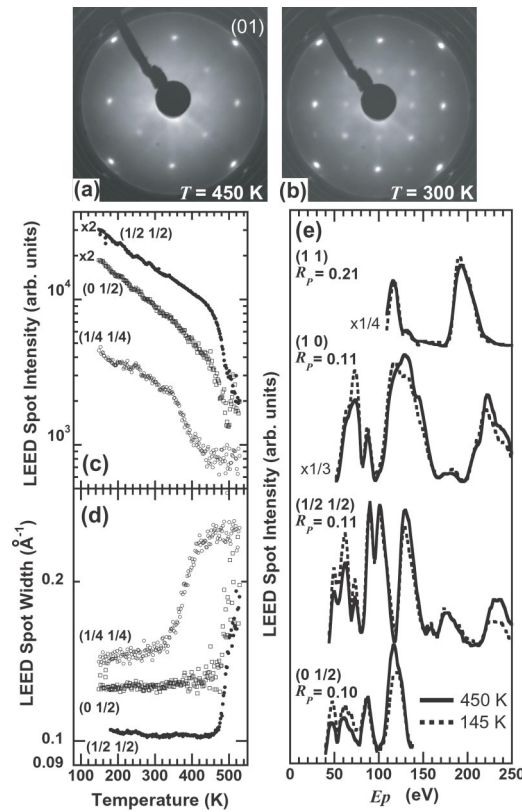


FIG. 1. LEED patterns with the primary energy of 60 eV of In(0.63 ML)/Cu(001) at (a) 450 K, (b) 300 K, and (c) integrated LEED intensities and (d) peak widths as a function of temperature. (e) LEED I - V curves measured at $T=450$ K (solid curves) and at $T=145$ K (dashed curves), which, for the sake of visual comparison, are normalized to those at 300 K by the Debye-Waller factor. The R_p values between the two curves are given.

e - ph coupling. We discuss the importance of the peculiar dimensionality of the metallic ultrathin films on metals.

Experiments were performed in several ultra-high vacuum chambers. A variable temperature STM (Oxford Instruments) was used to obtain atomic images in the constant-current (topographic) mode. The ARPES experiment was mainly performed at beam line 7.0 of the Advanced Light Source, Berkeley. The energy resolution was 50 meV. While the instrumental angular resolution was small ($\sim 0.1^\circ$), the systematic error in aligning spectra from different experimental runs was larger ($\sim 2^\circ$) in the experimental geometry employed. We therefore repeated the same experiment by using an high-angular-precision ($< 0.5^\circ$) electron spectrometer to confirm that the temperature-dependent behavior of the surface resonance band reported below is reproducible. The FS mapping was performed at beam line 7B of Photon Factory, Tsukuba, with the energy resolution of 200 meV and the angle of acceptance of $\pm 1^\circ$. The In/Cu(001) surface was prepared by deposition of 0.8–1.0 ML In and subsequent annealing at 550 K for 3 min, which gave homogeneous STM images and well-contrasted LEED patterns of the $(2\sqrt{2} \times 2\sqrt{2})R45^\circ [c(4 \times 4)]$ structure at room temperature. The coverage for this surface was determined previously to be 0.65 ± 0.04 ML.¹⁶ This surface is ultrastable against both

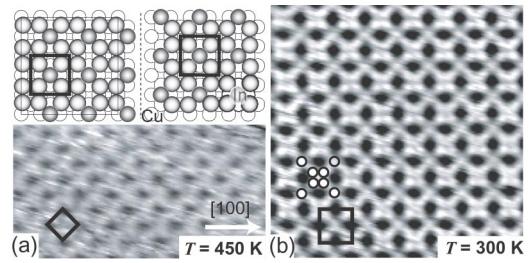


FIG. 2. STM images for (a) (2×2) ($V_s = -50$ meV, $I_t = 10$ nA, image size = $58 \times 58 \text{ \AA}^{-1}$), and (b) $(2\sqrt{2} \times 2\sqrt{2})R45^\circ$ ($V_s = -20$ meV, $I_t = 10$ nA, image size = $58 \times 58 \text{ \AA}^{-1}$). The inset in (a) shows the model for $(2\sqrt{2} \times 2\sqrt{2})R45^\circ$ domains in antiphase relation with each other.

contamination due to residual gasses and intermixing of In with substrate atoms. The Auger electron spectroscopy shows no detectable changes of In LMM or Cu MVV Auger signals for heating-cooling cycles, and LEED, STM, or ARPES shows no indication of contamination or the degradation of structural order even after several days of experiments so long as the temperature is maintained below ~ 450 K.

The surface exhibits a sharp and well-contrasted $(2\sqrt{2} \times 2\sqrt{2})R45^\circ$ LEED pattern at 300 K as shown in Fig. 1(a). Upon heating, the surface undergoes a transition to a (2×2) phase, whose LEED pattern is shown in Fig. 1(b). The intensity of the $(1/4 \ 1/4)$ spot due to the $(2\sqrt{2} \times 2\sqrt{2})R45^\circ$ domains exhibits a steep decrease in concomitant with the rapid increase of the width as shown in Figs. 1(c), 1(d). The transition temperature is estimated to be $T_c = 405$ K. Upon further heating, the surface successively transforms at ~ 500 K to a (1×1) phase, as indicated by the behavior of the $(1/2)$ th order spots due to the (2×2) symmetry. The (1×1) LEED pattern is associated with high background, indicating that the surface is disordered.

Figure 2(a) shows a high-resolution STM image taken at 450 K, which exhibits a square-net structure with its unit length of $\sim 5 \text{ \AA}$ along the $[110]$ direction, while the individual atoms are not resolved. The structure is consistent with the (2×2) periodicity observed by LEED. At 300 K, STM shows a $(2\sqrt{2} \times 2\sqrt{2})R45^\circ$ periodicity, as shown in Fig. 2(b), where the “monomers” and “tetramers” of protrusions are arranged regularly.

The In coverage, 0.65 ± 0.04 ML, is in good agreement with the square $(2\sqrt{2} \times 2\sqrt{2})R45^\circ$ periodicity. The density of the protrusions in the STM image is $5/8$, resulting in a nominal coverage of 0.63 ML. On the other hand, *this coverage is not consistent with any long-range orders of a periodicity of (2×2) , which should be associated with a coverage of $n/4$ ML with n an integer.* An extensive STM observation at 450 K indicates that the surface is uniformly covered with the (2×2) -In layer, which gives rise to the STM image shown in Fig. 2(a). In order to compare quantitatively the local structure of the (2×2) and $(2\sqrt{2} \times 2\sqrt{2})R45^\circ$ phases, we took LEED intensity versus acceleration voltage (I - V) curves for integer- and half-integer-order spots at 150 and 450 K [Fig. 1(f)]. The peak positions

are in a good agreement between HT and LT surfaces. The very small Pendry's reliability factor,¹⁷ $R_p=0.13$ between two surfaces suggests that the local structures within the (2×2) unit cell in the two phases are essentially the same.

The above arguments suggest the disordered nature of the HT phase. The (2×2) STM images should be due to the time average of the temporally fluctuating surface. A possible model for the "disorder" is as follows. Figure 2(a) shows two $(2\sqrt{2} \times 2\sqrt{2})R45^\circ$ domains in antiphase relation with each other. If the structure fluctuates between these two configurations in a time scale shorter than that of the STM scanning, the resulting image would be the one where the images from two antiphase domains are superimposed. The image shown in Fig. 2(a) may be understood as due to such a dynamical fluctuation. On the other hand, if the spatial extents of the $(2\sqrt{2} \times 2\sqrt{2})R45^\circ$ domains are much smaller than the transfer width of LEED ($\sim 100 \text{ \AA}$), one should observe the (2×2) LEED pattern due to the interference between antiphase domains.

In the paragraphs below, the electronic origin of the phase transition is discussed. In Fig. 3(a), we show the 2D FS mapped at 450 K. The outer circlelike feature comes from the In derived surface resonances,¹⁶ while the inner features are due to the emission from the bulk Cu. The 2D FS is constituted of nearly free-electron-like surface resonance bands (lower band S_1 and upper band S'_1).^{5,16} While the surface has a (2×2) periodicity, the spectral weight is concentrated on the extended-zone-scheme dispersion due to a photoemission structure factor effect.¹⁸

Figure 3(c) shows ARPES spectra along $\bar{\Gamma}-\bar{M}$, where the S_1 band crosses the Fermi level at 1.44 \AA^{-1} both in the HT and in the LT phases. Along $\bar{\Gamma}-\bar{M}$ no significant differences in the band structure are observed during the transition. Along line (d), the S_1 band crosses E_F at 450 K, while in the LT phase the S_1 band backfolds below E_F towards higher binding energies. While the $[100]$ component of the HT-phase Fermi wave vector, $k_{F,x}=1.35 \text{ \AA}^{-1}$, deviates slightly from the surface Brillouin zone (SBZ) boundary ($k_x=1.30 \text{ \AA}^{-1}$) of $(2\sqrt{2} \times 2\sqrt{2})R45^\circ$, the backfolding point at 140 K lies on the SBZ boundary. Along line (e), where $k_{F,x}$ of the HT phase coincides closely with the $(2\sqrt{2} \times 2\sqrt{2})R45^\circ$ SBZ boundary, the ARPES spectra taken for the LT phase also show backfolding on the $(2\sqrt{2} \times 2\sqrt{2})R45^\circ$ SBZ boundary. The region where the energy gap at E_F is formed in the LT phase is restricted around lines (d) and (e), where the $(2\sqrt{2} \times 2\sqrt{2})R45^\circ$ SBZ boundary and the HT FS are located within $\sim 0.1 \text{ \AA}^{-1}$. For the other part of the $(2\sqrt{2} \times 2\sqrt{2})R45^\circ$ SBZ boundary closer to $\bar{\Gamma}-\bar{M}$, only a very small band gap ($< 100 \text{ meV}$) is formed below E_F . Thus, the ARPES results indicate that the transition is associated with the partial nesting of the 2D FS and hence is categorized into the Peierls-type CDW transition. The formation of the commensurate CDW state rather than the incommensurate one indicates that the e -ph matrix element effects play a significant role.^{19,20} A weak metallic band is also seen below the transition temperature along lines (d) and (e), which may be due to the local (2×2) domains remnant on the surface.

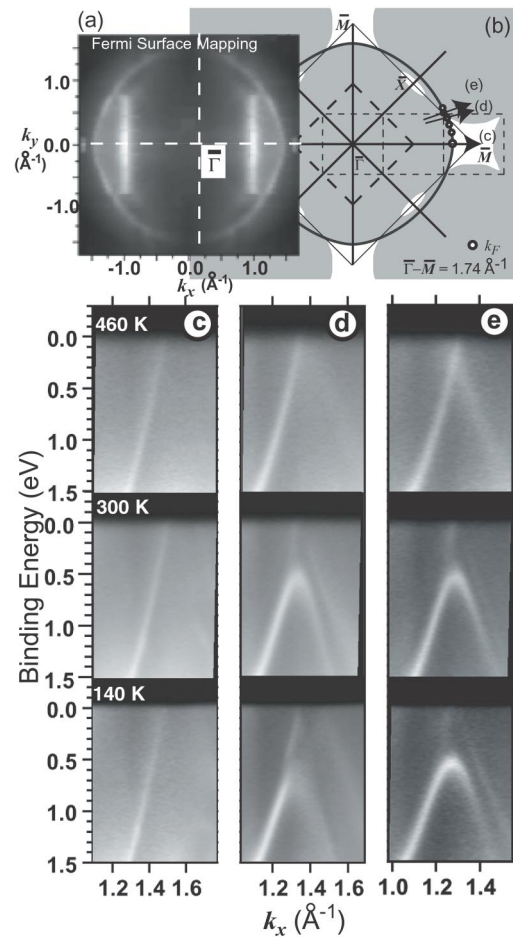


FIG. 3. (a) Fermi surface for the (2×2) surface mapped at 450 K with $h\nu=22.8 \text{ eV}$ and the photon polarization in a (010) plane, and (b) its schematic drawing (gray line) and SBZ for 1×1 (solid), (2×2) (dashed), and $(2\sqrt{2} \times 2\sqrt{2})R45^\circ$ (dotted lines). The arrows (c)–(e) are the path along which the spectra shown in the bottom were taken. (c)–(e) ARPES band mappings taken at 140, 300, and 460 K with $h\nu=80.0 \text{ eV}$ along the paths indicated above.

The band gap 2Δ serves as the order parameter of WCDW transitions. According to the WCDW theory, the temperature dependence of Δ is described by the same equation as that given by the BCS theory for the superconductivity. At temperatures well below T_c , Δ is almost independent of the temperature and gradually approaches zero as $T \rightarrow T_c$ from below. On the other hand, in the SCDW regime, the lattice entropy dominates the temperature dependence of the free energy and hence the band gap Δ is not considered as an order parameter. In this case, Δ corresponds to the bonding-antibonding splitting of the local chemical bonds and hence is almost constant up to a much higher transition temperature $T_o > T_c$.^{4,6} For $T > T_o$, one expects to find a perfect long-range order with an ungapped spectrum, while at intermediate temperatures, one expects a gapped spectrum with short-range spatial and temporal lattice fluctuations. This order-disorder-order transition described by the SCDW theory is supported by our LEED and STM results.

Our temperature-dependent ARPES results contradict this picture, however. The spectra measured at 460 K show that

the band gap diminishes along line (d) and a much reduced band gap of ~ 0.2 eV is observed along line (e). (In the latter case it is not clear if there is actually a gap, since the spectral weight is rather high even at E_F at the backfolding point.) The k width of the metallic S_1 band at 460 K is rather small ($\sim 0.05 \text{ \AA}^{-1}$), indicating that the coherence length exceeds 100 \AA . The facts that the large band gap ($2\Delta \sim 1.2$ eV) formed in the LT phase and that the gap diminishes above T_c suggest that a considerable electronic energy gain is associated with the CDW formation and that, in addition to the lattice entropy, the electronic entropy contributes significantly to the temperature dependence of the free energy. This situation is qualitatively in much better accordance with the WCDW picture.

We believe that the seemingly conflicting results provide an evidence for the dual nature of a 2D CDW phase transition driven concertedly by electronic and lattice entropies. Note that the present case cannot be considered as “intermediate” between strong- and weak-coupling limits, because in this case the gapping should be incomplete at the structural transition temperature. It should be considered that two mechanisms coexist in the present surface. The nature of the transition is also seen in the temperature dependence of the 2Δ value below T_c . At 140 K, the binding energy of the lower band (S_1) maximum, δ_l , is slightly k dependent and varies from 0.59 to 0.63 eV, and δ_l decreases to 0.53–0.54 eV at 300 K. The ratio $\delta_l(300 \text{ K})/\delta_l(140 \text{ K}) \sim 0.9$ can be compared with that expected for 2Δ from the WCDW theory, 0.78, for $T_c = 405$ K. The deviation may be addressed to the interplay of the electronic entropy with the lattice entropy.

Let us finally discuss the effects of the peculiar dimen-

sionality of the present system. For ultrathin films on *metal* surfaces, the electron system of the substrate should play a role. For bulk materials, irrespective of whether these have quasi-1D or quasi-2D FS, the transition is characterized by a single energy parameter 2Δ , which determines the condensation energy of CDW's and governs the electronic entropy of the CDW phases. The former is true also in metal-surface systems. However, the electronic excitation from the bulk band near E_F to the resonance band above the gap should occur in these systems, which increases the electronic entropy at temperatures much below that where the excitations across the CDW gap (2Δ) are possible. While the energy separation δ_u between E_F and the upper band minimum is, at the moment, not known in the present system, it can be much smaller than Δ because the nesting vector is deviated from the Fermi wave vector. Thus, it is possible to hypothesize that the dual nature of the CDW transition in the present system is a consequence of the coexistence of two energy parameters: 2Δ and δ_u ; the former governs the CDW enthalpy and the latter the electronic entropy. Further experimental examinations, particularly for the critical behaviors of structural and electronic properties near T_c , are desirable in order to examine the hypothesis.

A part of the work was performed under the approval of the Photon Factory Program Advisory Committee (Grant No. PF-PAC No. 2001G017). The Advanced Light Source is supported by the Director, Office of Science, Office of Basic Energy Sciences, Materials Sciences Division, of the U.S. Department of Energy under Contract No. DE-AC03-76SF00098 at Lawrence Berkeley National Laboratory. HWY was supported by KOSEF through ASSRC.

*Present address: Institute for Molecular Science, Okazaki 444-8585, Japan.

†Email address: aruga@kuchem.kyoto-u.ac.jp

¹J.M. Carpinelli, H.H. Weitering, E.W. Plummer, and R. Stumpf, *Nature* (London) **381**, 398 (1996); J.M. Carpinelli, H.H. Weitering, M. Bartkowiak, R. Stumpf, and E.W. Plummer, *Phys. Rev. Lett.* **79**, 2859 (1997).

²G. Grüner, *Density Waves in Solids* (Addison-Wesley, Reading, MA, 1994).

³S. Kagoshima, H. Nagasawa, and T. Sanbongi, *One-Dimensional Conductors* (Springer, Berlin, 1988).

⁴E. Tosatti, in *Electronic Surface States and Interface States on Metallic Systems*, edited by E. Bertel and M. Donath (World Scientific, Singapore, 1995), p. 67.

⁵T. Aruga, *J. Phys.: Condens. Matter* **35**, 8393 (2002).

⁶W.L. McMillan, *Phys. Rev. B* **16**, 643 (1977).

⁷E. Tosatti, in *Modern Trends in the Theory of Condensed Matter*, edited by A. Pekalski and J. Przystawa (Springer-Verlag, Berlin, 1980), p. 501.

⁸G.-H. Gweon, J.D. Denlinger, J.A. Clack, J.W. Allen, C.G. Olson, E. DiMasi, M.C. Aronson, B. Foran, and S. Lee, *Phys. Rev. Lett.* **81**, 886 (1998).

⁹R. Liu, C.G. Olson, W.C. Tonjes, and R.F. Frindt, *Phys. Rev. Lett.* **80**, 5762 (1998).

¹⁰Th. Straub, Th. Finteis, R. Claessen, P. Steiner, S. Hufner, P. Blaha, C.S. Oglesby, and E. Bucher, *Phys. Rev. Lett.* **82**, 4504 (1999).

¹¹H.W. Yeom, S. Takeda, E. Rotenberg, I. Matsuda, K. Horikoshi, J. Schaefer, C.M. Lee, S.D. Kevan, T. Ohta, T. Nagao, and S. Hasegawa, *Phys. Rev. Lett.* **82**, 4898 (1999).

¹²T.E. Kidd, T. Miller, M.Y. Chou, and T.-C. Chiang, *Phys. Rev. Lett.* **85**, 3684 (2000).

¹³R. Liu, W.C. Tonjes, V.A. Greanya, C.G. Olson, and R.F. Frindt, *Phys. Rev. B* **61**, 5212 (2000).

¹⁴T. Nakagawa, G.I. Boishin, H. Fujioka, H.W. Yeom, I. Matsuda, N. Takagi, M. Nishijima, and T. Aruga, *Phys. Rev. Lett.* **86**, 854 (2001).

¹⁵K. Swamy, A. Menzel, R. Beer, and E. Bertel, *Phys. Rev. Lett.* **86**, 1299 (2001).

¹⁶T. Nakagawa, S. Mitsushima, H. Okuyama, M. Nishijima, and T. Aruga, *Phys. Rev. B* **66**, 085402 (2002).

¹⁷J.B. Pendry, *J. Phys. C* **13**, 937 (1980).

¹⁸J. Voit, L. Perfetti, F. Zwick, H. Berger, G. Margaritondo, G. Grüner, H. Höchst, and M. Grioni, *Science* (Washington, DC, U.S.) **290**, 501 (2000).

¹⁹I. Terakura, K. Terakura, and N. Hamada, *Surf. Sci.* **103**, 103 (1981).

²⁰X.W. Wang, C.T. Chan, K.M. Ho, and W. Weber, *Phys. Rev. Lett.* **60**, 2066 (1988).